RSC Advances

PAPER

View Article Online
View Journal | View Issue

Cite this: *RSC Adv.*, 2024, **14**, 5406

Surface engineering of carbon microspheres with nanoceria wrapped on MWCNTs: a dual electrocatalyst for simultaneous monitoring of molnupiravir and paracetamol†

Yahya S. Alqahtani,[a] Ashraf M. Mahmoud,[a] Mohamed M. El-Wekil [b] and Hossieny Ibrahim *[cd]

Received 27th November 2023
Accepted 24th January 2024

DOI: 10.1039/d3ra08098f

rsc.li/rsc-advances

In the present study, nanoceria-decorated MWCNTs (CeNPs@MWCNTs) were synthesized using a simple and inexpensive process. Molnupiravir (MPV) has gained considerable attention in recent years due to the infection of severe acute respiratory syndrome coronavirus-2 (SARS-CoV-2). Since some people infected with COVID-19 experience fever and headaches, paracetamol (PCM) has been prescribed to relieve these symptoms. Therefore, there is an urgent need to monitor and detect these drugs simultaneously in pharmaceutical and biological samples. In this regard, we developed a novel sensor based on nanoceria-loaded MWCNTs (CeNPs@MWCNTs) for simultaneous monitoring of MPV and PCM. The incorporation of CeNPs@MWCNTs electrocatalyst into a glassy carbon microsphere fluorolube oil paste electrode (GCMFE) creates more active sites, which increase the surface area, electrocatalytic ability, and electron transfer efficiency. Interestingly, CeNPs@MWCNTs modified GCMFE demonstrated excellent detection limits (6.0 nM, 8.6 nM), linear ranges (5.0–5120 nM, 8.0–4162 nM), and sensitivities (78.6, 94.3 μA μM^{-1} cm^{-2}) for simultaneous detection of MPV and PCM. The developed CeNPs@MWCNTs electrocatalyst modified GCMFE exhibited good repeatability, anti-interference capability, stability, and real-time analysis with good recovery results, which clearly indicates that it can be used for real-time industrial applications.

Introduction

Monitoring of drugs is a significant aspect in pharmaceuticals, healthcare, and biological samples for the controlled analysis of drug dosages. Antiviral drugs have gained considerable attention in recent years due to the severe acute respiratory syndrome coronavirus-2 (SARS-CoV-2) infection. Molnupiravir (MPV), an oral ribonucleoside analog with broad-spectrum antiviral activity, is a prodrug of the synthetic nucleoside derivative *N*4-hydroxycytidine (NHC). Clinical trials have shown that treatment with MPV reduces deaths and hospitalizations in patients with COVID-19 infections.[1,2] Paracetamol (PCM), a well-known antipyretic and analgesic compound, is extensively used for the treatment of fever, cough, cold, and pain including muscular ache, chronic pain, headache, backache and toothache.[3–5] Moreover, PCM has been frequently used to reduce fever during the COVID-19 pandemic.[6–8] Abnormal MPV and PCM levels in the body can affect the immune system, which may lead to some diseases. Therefore, there is an urgent need to simultaneously monitor and detect these two drugs in human biological samples.

Although a wide range of techniques are available, the detection technique with factors, including simple, easier handling/operation, and quick and sensitive detection, is the most preferable one.[9–11] The electrochemical sensor covers all these features; hence, it is utilized to simultaneously monitor and measure MPV and PCM, particularly in human biological fluids and pharmaceutical products. Many methods are described in the literature that can measure MPV or PCM using HPLC,[12–14] UV spectrophotometry,[15,16] and electrochemical methods.[17–28] However, except for electrochemical methods, all other analytical methods are complicated, tedious, time-consuming, and expensive. Electrochemical methods are time-saving, simple, real-time, user-friendly, and economically worthwhile.

The implementation of an electrochemical sensor for the simultaneous assay of MPV and PCM requires electrode modification. The beneficial factors of the modified electrodes include improved sensitivity, higher transfer of electrons,

[a]*Department of Pharmaceutical Chemistry, College of Pharmacy, Najran University, Najran, Saudi Arabia*

[b]*Department of Pharmaceutical Analytical Chemistry, Faculty of Pharmacy, Assiut University, Assiut, Egypt*

[c]*Department of Chemistry, Faculty of Science, Assiut University, Assiut 71516, Egypt. E-mail: Hossieny.Ibrahim@aun.edu.eg*

[d]*School of Biotechnology, Badr University in Assiut, Assiut 2014101, Egypt*

† Electronic supplementary information (ESI) available. See DOI: https://doi.org/10.1039/d3ra08098f

enhanced conductivity, and surface area. A huge variety of materials, such as metal oxide nanoparticles and carbon-based composites, are available.[29–32] In recent years, nanoparticle-based metal oxide electrochemical sensors have garnered a great deal of interest in electrocatalysis.[33–35] Due to its unique properties, nano-CeO_2 (CeNPs) has been applied in various fields, including supercapacitors, solar cells, photocatalysis, and sensors.[36–38] Nevertheless, it has been observed that CeNPs tend to aggregate, leading to a decrease in the electrocatalytic activity. Furthermore, the electrocatalytic efficacy of CeNPs is limited by their comparatively low conductivity. Multi-walled carbon nanotubes (MWCNTs) exhibit high electron transfer efficiency and mechanical stability and are therefore suitable conductive substrates for flexible sensors.[39] Therefore, the combination of MWCNTs and CeNPs is an effective approach for increasing the conductivity and promoting the electrocatalytic activity of CeNPs.

Carbon, in many respects, is an ideal electrode substrate owing to its wide anodic potential range, low residual current, chemical inertness, and low cost. Moreover, carbon electrodes exhibit a fast response time and can be easily fabricated in different configurations and sizes. Among the family of carbon, glassy carbon microspheres (GCMs) are the most popular electrode material, offering attractive electrochemical reactivity, negligible porosity, and good mechanical rigidity.[29,34] Glassy carbon paste electrodes (GCPEs) combine the attractive properties of composite electrodes and glassy carbon because the preparation of these electrodes includes the mixing of GCMs with organic-pasting liquid. GCPEs offer high electrochemical reactivity, a wide accessible potential window; low background current; are easy to prepare, modify, and renew; and are inexpensive.[40,41]

In this work, for the first time, we developed a glassy carbon microsphere fluorolube oil paste electrode (GCMFE) modified with CeNPs@MWCNTs electro-catalyst for simultaneous determination of MPV and PCM. To the best of our knowledge, simultaneous determination of the anti-coronavirus MPV and PCM has not been carried out. The CeNPs@MWCNTs electrocatalyst-modified GCMFE exhibits excellent electrochemical sensing capability for simultaneous detection of MPV and PCM in human biological fluids and pharmaceutical samples, which reveals the potential practical applications of the CeNPs@MWCNTs electrocatalyst.

Experimental

Detailed information regarding the chemicals, reagents, instruments, and preparation of the real samples can be found in the ESI.†

Synthesis of CeNPs and CeNPs@MWCNTs electrocatalyst

Detailed information regarding the synthesis procedure of CeNPs can be found in the ESI.† CeNPs@MWCNTs were prepared by mixing CeNPs and MWCNTs (1 : 1, 1 : 2, 2 : 1 w/w) in ethanol. These mixtures were subjected to sonication for 1 h and they were then transferred to a glass Petri dish and heated (70 °C) for 24 h to evaporate the ethanol. Finally, the dry black solid CeNPs@MWCNTs electrocatalyst was obtained.

Preparation of the electrodes

A glassy carbon microsphere paraffin oil paste electrode (GCMPE) was fabricated by blending paraffin oil and GCM (80 : 20 w/w). A glassy carbon microsphere fluorolube oil paste electrode (GCMFE) was then developed using the same procedure, however, with fluorolube oil rather than paraffin oil. The produced paste was placed into a Teflon tube ($A_G = 0.07$ cm^2). The CeNPs@MWCNTs electrocatalyst modified GCMFEs

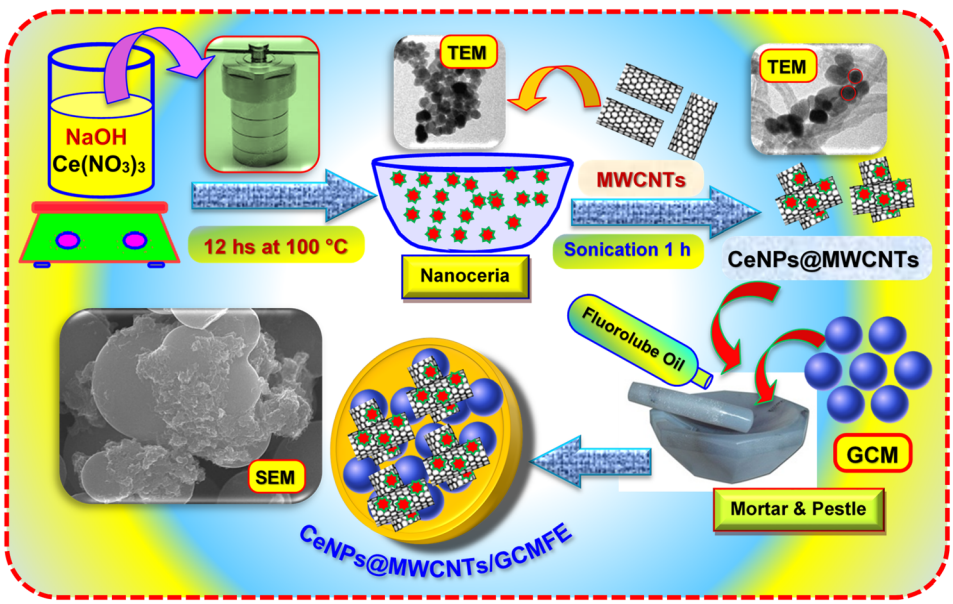

Scheme 1 Schematic diagram of preparation process of CeNPs@MWCNTs modified GCMFE.

(CeNPs@MWCNTs/GCMFE) were fabricated by blending (5, 10, 15, and 20 mg) of CeNPs@MWCNTs with GCM and 20% fluorolube oil. Similarly, CeNPs/GCMFE and MWCNTs/GCMFE were prepared (Scheme 1).

Ethical statement

All experiments were performed in compliance with the relevant laws and Assiut University's guidelines. These studies were approved by the ethics committees of Assiut Medical University – Joint Institutional Review Board. All of the subjects signed an informed consent form before the examination.

Results and discussion

Morphological studies

The crystal structures of MWCNTs, CeO_2 nanoparticles (CeNPs), and CeNPs@MWCNTs were studied using XRD analysis, as shown in Fig. S1A.† The XRD pattern of MWCNTs demonstrated an intense diffraction peak around $2\theta = 25.32°$ and a low intense diffraction peak around 41.67°, which are ascribed to (002) and (100), respectively. This result shows that the MWCNTs are well graphitized (Fig. S1A,† curve a). As expected, CeNPs display sharp diffraction peaks at (111), (200), (220), (311), (222), and (400) for the face-centered cubic CeO_2. The XRD patterns agreed well with the standard CeO_2 crystal lattice (JCPDS card No. 04-013-4459) (Fig. S1A,† curve b). Fig. S1A† (curve c) shows the XRD profiles of CeNPs@MWCNTs with sharp diffraction peaks at (111), (200), (220), (311), (222), and (400) for the face-centered cubic CeO_2. Notably, the XRD peaks of MWCNTs disappeared from the CeNPs@MWCNTs nanocomposite. This may be attributed to the high degree of CeNPs wrapped on MWCNTs. Furthermore, MWCNTs are used to support metal oxides (CeNPs) to enhance the catalytic properties of MWCNT composites through the strong interactions between them.[42] Fig. S1B† shows the TEM image of the CeNPs material, indicating that it consists of a large number of particles. The magnified HR-TEM image shown in Fig. S1C† shows the lattice spacing of about 0.34 nm, *hkl* (111), and 0.29 nm, *hkl* (200), which are typical for cubic CeO_2 structures. The histogram of Fig. S1D† reveals the particle size distribution with an average diameter of 12 nm.

The surface morphology of the CeNPs/MWCNTs electrocatalyst (2 : 1 w/w) was examined by SEM and TEM techniques (Fig. 1A and B). As can be seen, most of the MWCNTs are decorated with CeNPs, which provides a large active surface area. The surface morphology of GCMFE and CeNPs@MWCNTs electrocatalyst-modified GCMFE was studied by SEM. Fig. 1C shows highly packed non-porous microspheres and no topographic features characterize the surface of the GCM-fluorolube oil electrode (GCMFE); however, Fig. 1D displays how the CeNPs@MWCNTs electrocatalyst helps to wire each GCM into an electrical contact and to bind and stabilize the microspheres within the film structure.

Electrochemical analysis

The electrochemical impedance spectroscopy (EIS) performance of the bare GCMPE and fabricated electrodes were

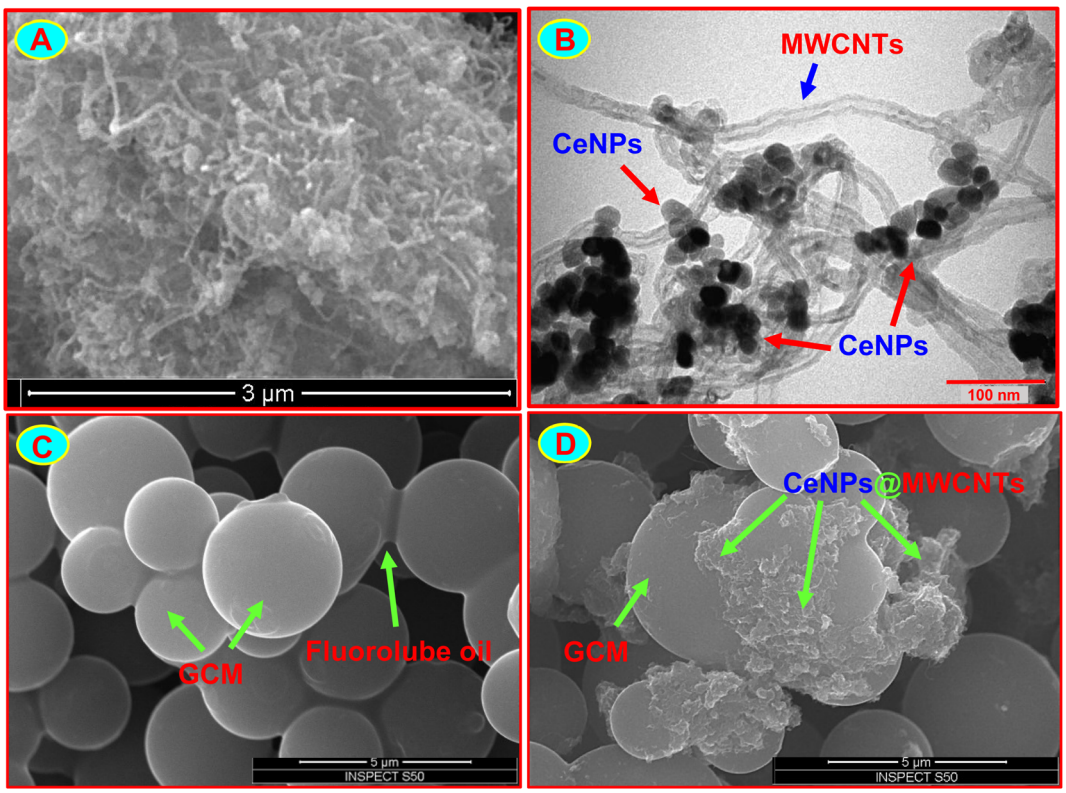

Fig. 1 SEM (A) and TEM (B) images of CeNPs@MWCNTs. SEM images of GCMFE (C) and CeNPs@MWCNTs/GCMFE (D).

evaluated in a three-electrode system containing 5 mM $K_3Fe(CN)_6/K_4Fe(CN)_6$ and 0.1 M KCl (Fig. 2A). It was observed that GCMFE presented a charge transfer resistance (R_{ct} = 2225 ± 46 Ω) lower than GCMPE (R_{ct} = 3025 ± 53 Ω), which may be related to the presence of fluorolube oil, accelerating the electronic transfer. When modified by CeNPs, R_{ct} considerably decreased to 1438 ± 38 Ω. After the application of the MWCNTs nanomaterial to the electrode surface, the resistance decreased to 963 ± 24 Ω, which indicates that the presence of MWCNTs may facilitate the transfer of charge and improve the conductivity of the electrode. Among the electrode materials, CeNPs@MWCNTs modified GCMFE exhibits the smallest R_{ct} value (225 ± 13 Ω). This result is mainly due to the benefits of the synergistic effect of CeNPs with large specific surface areas and MWCNTs with high electrical conductivity.

Characterization of the modified electrodes was performed by cyclic voltammetry (CV) and the obtained data are shown in Fig. 2B. After the GCMFE was incorporated into CeNPs, MWCNTs, and CeNPs@MWCNTs nanomaterials, the potential difference (ΔE_p) between the redox peaks of the $K_3Fe(CN)_6/K_4Fe(CN)_6$ decreased to 223, 198 and 161 mV, respectively, accompanied by the peak current increment. This indicates that the CeNPs@MWCNTs/GCMFE have higher catalytic ability than bare GCMPE and CeNPs, MWCNTs modified GCMFEs. The EIS data agreed with the CV and demonstrated the successful construction of the electrochemical sensor.

The values of the charge transfer rate constant (k_{et}) for the modified electrodes were calculated from R_{ct} *via* eqn (1):[43]

$$k_{et} = RT/F^2R_{ct}AC \quad (1)$$

The k_{et} values for GCMPE, GCMFE, CeNPs/GCMFE, MWCNTs/GCMFE and CeNPs@MWCNTs/GCMFE were measured as 2.5 × 10^{-4}, 3.4 × 10^{-4}, 6.0 × 10^{-4}, 8.0 × 10^{-4}, and 33.8 × 10^{-4} cm s^{-1}, respectively. The larger k_{et} value of the CeNPs@MWCNT-modified GCMFE compared with those of the other electrodes showed highly efficient electron transport at the electrolyte/electrode interface of CeNPs@MWCNTs/GCMFE.[44] Moreover, to estimate the electrocatalytic ability, the exchange current (I_0) is frequently measured using eqn (2):[45]

$$I_0 = RT/nFR_{ct} \quad (2)$$

The I_0 values calculated for GCMPE, GCMFE, CeNPs/GCMFE, MWCNTs/GCMFE, and CeNPs@MWCNTs/GCMFE were 8.5, 11.5, 17.8, 26.7, and 114.0 μA cm^{-1}, respectively, which confirmed the higher electrocatalytic activity of the CeNPs@MWCNTs electrocatalyst. Effective surface area (Fig. S2† and 2C) was calculated using Randles–Sevcik eqn (3).[46,47]

$$I_{pa} = (2.69 \times 10^5)n^{3/2}A_{eff}D^{1/2}\nu^{1/2}C \quad (3)$$

where A_{eff} represents the effective surface area, I_{pa} represents the anodic peak current, n represents the number of electrons transferred in the redox reaction (n = 1), C represents the concentration of $[Fe(CN)_6]^{3-/4-}$ (mol cm^{-3}), and D represents the diffusion coefficient of the ferricyanide solution (7.6 × 10^{-6} cm^2 s^{-1}). The obtained A_{eff} values increased in the following order: CeNPs@MWCNTs/GCMFE (0.86 ± 0.022 cm^2) > MWCNTs/GCMFE (0.43 ± 0.017 cm^2) > CeNPs/GCMFE (0.33 ± 0.014 cm^2) > GCMFE (0.25 ± 0.010 cm^2) > GCMPE (0.19 ± 0.006 cm^2). Finally, CeNPs@MWCNTs/GCMFE possessed the most A_{eff} among the electrodes, indicating that the CeNPs@MWCNTs electrocatalyst-modified GCMFE exhibited improved electrocatalytic performance. Furthermore, the surface roughness factor ($R_f = A_{eff}/A_G$) assessed for CeNPs@MWCNTs/GCMFE (R_f = 12.6) was larger than that of GCMPE (R_f = 2.7). The results show that the CeNPs@MWCNTs electrocatalyst has a higher surface area and therefore provides more catalytic reaction sites, thereby accelerating the electron mass transfer efficiency.

Electro-catalytic oxidation of MPV and PCM

CVs of the unmodified and differently modified working electrodes toward MPV and PCM were examined in the Britton–Robinson buffer (BRB). The oxidation peak of MPV at 440 mV was relatively weak and broad at bare GCMPE, indicating the lower electrocatalytic activity of the unmodified electrode (Fig. 3A). Compared with the bare GCMPE, the oxidative peak negatively shifted to 338 mV when CeNPs@MWCNTs/GCMFE was used. Importantly, the peak current observed at the CeNPs@MWCNTs electrocatalyst-modified GCMFE was almost 5 times that of the unmodified GCMPE, which can be attributed to the electrocatalytic performance of CeNPs@MWCNTs/GCMFE on the electro-oxidation of MPV. Then, the electrochemical performances

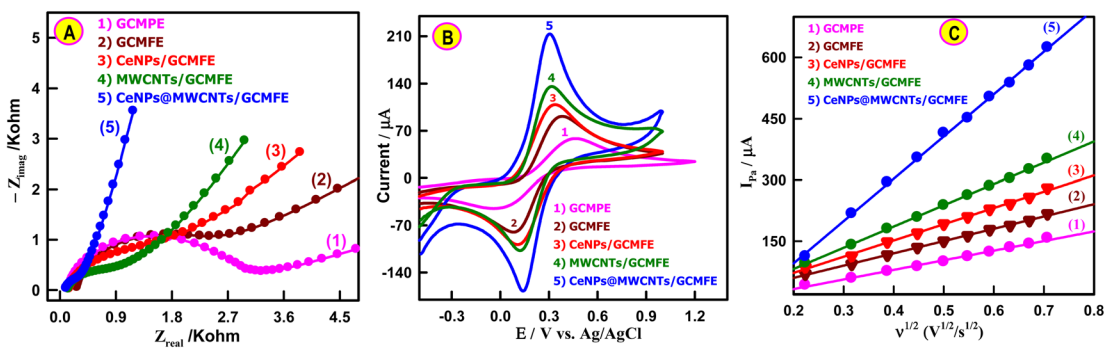

Fig. 2 (A) Nyquist plots and (B) CVs of (1) GCMPE, (2) GCMFE, (3) CeNPs/GCMFE, (4) MWCNTs/GCMFE and (5) CeNPs@MWCNTs/GCMFE in 5 mM $[Fe(CN)_6]^{3-}/[Fe(CN)_6]^{4-}$ (1 : 1 mixture) solution containing 0.1 M KCl at a scan rate of 100 mV s^{-1}. (C) Plot of I_{Pa} *vs.* ν.

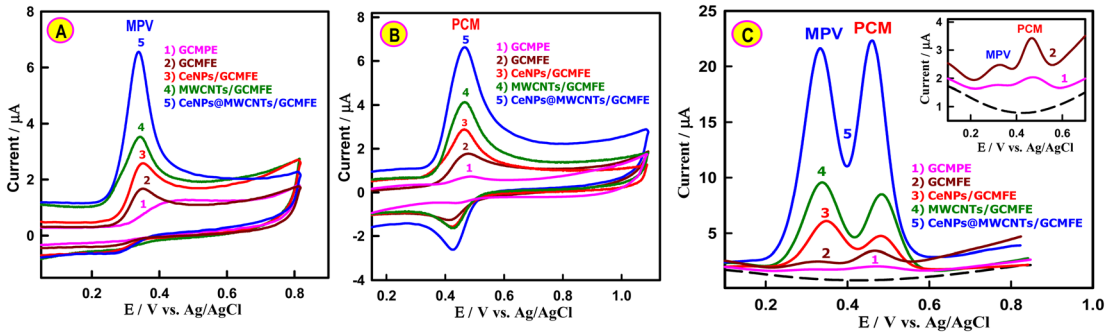

Fig. 3 CVs of (A) 1.5 μM MPV and of 1.2 μM PCM (B) in BRB solution of pH 6.0 obtained at (1) GCMPE, (2) GCMFE, (3) CeNPs/GCMFE, (4) MWCNTs/GCMFE and (5) CeNPs@MWCNTs/GCMFE. (C) AdS-SW voltammograms at (1) GCMPE, (2) GCMFE, (3) CeNPs/GCMFE, (4) MWCNTs/GCMFE, and (5) CeNPs@MWCNTs/GCMFE in BRB solution (pH 6.0) containing 2.6 μM MPV and 2.0 μM PCM.

of PCM at bare GCMPE, GCMFE, CeNPs/GCMFE, MWCNTs/GCMFE, and CeNPs@MWCNTs/GCMFE were investigated (Fig. 3B). Comparing the related CVs, the bare GCMPE demonstrates a pair of weak redox peaks, while CeNPs@MWCNTs/GCMFE possesses a pair of well-defined redox peaks with higher current responses. The CeNPs@MWCNTs/GCMFE sensor is more responsive to PCM compared to the unmodified GCMPE owing to its excellent electroactive area.

In addition, the simultaneous electrocatalytic responses of 2.6 μM MPV and 2.0 μM PCM were explored by adsorptive stripping square-wave voltammetry (AdS-SWV) in BRB solution of pH 6.0. At the bare GCMPE (inset of Fig. 3C), the MPV and PCM exhibited two small anodic peaks compared to the GCMFE, suggesting low conductivity and slow electron transfer of paraffin oil as a binder. However, after incorporating CeNPs or MWCNTs into GCMFE, the oxidation peak currents of MPV and PCM improved (Fig. 3C, curves 3 and 4). Interestingly, the fabricated CeNPs@MWCNTs/GCMFE showed considerably higher MPV and PCM oxidation currents (12-fold and 11.2-fold, respectively) compared to bare GCMPE (Fig. 3C, curve 5). This significant change was mainly attributed to the large electroactive surface area of the nanostructured CeNPs@MWCNTs that facilitated the contact of the electrolyte with the electrode surface, thus improving the detection of MPV and PCM by strengthening their absorption on the electrode.

Optimization studies

To acquire the strongest signal response and the highest sensitivity for the detection of MPV and PCM, we optimized the experimental conditions using the AdS-SWV method, including the pH of the BRB solution, supporting electrolyte and mass ratio of CeNPs@MWCNTs electrocatalyst to GCM. The effect of the pH range of the buffer, from 3 to 8, on peak currents and potentials of the two analytes in the BRB solution containing 2.6 μM MPV and 2.0 μM PCM on CeNPs@MWCNTs/GCMFE was investigated. The voltammograms displayed two oxidation peaks at all pH values (Fig. S3A†). When pH was 6.0, the current responses of MPV and PCM had the maximum value; therefore, a BRB solution with a pH of 6.0 was used for the experiments. Furthermore, the peak potential (E_{pa}) gradually moved in a more negative direction with the increase of pH, which indicates that the proton participates in the redox reaction process. The regression equations are provided as part of the analysis, $E_{Pa,MPV}$ (V) = 0.71–0.061 pH, R^2 = 0.9981 and $E_{Pa,PCM}$ (V) = 0.9–0.064 pH, R^2 = 0.9986 (Fig. S3B and C†). The slope values in these equations were 61 and 64 mV pH^{-1}, which were almost consistent with the Nernstian standard value of 59.0 mV pH^{-1}. This result indicated that the electro-oxidation process of MPV and PCM on CeNPs@MWCNTs electrocatalyst-modified GCMFE involved an equal number of electrons and protons. Detailed information regarding the influence of the supporting electrolyte, mass ratio of CeNPs@MWCNTs electrocatalyst to GCM, and AdS-SWV parameters can be found in the ESI.†

Impact of the scan rate

The study of electrode kinetic characteristics can be realized by researching the scanning rate. Fig. S6A and D† show the CV curves of CeNPs@MWCNTs modified GCMFE with the scanning rate increasing from 50 to 400 mV s^{-1} in MPV and PCM, respectively. The illustrations show the linear relationship between I_{pa} and the scan rate (ν) (Fig. S6B and E†). The linear regression equations were: I_{Pa} (μA) = 2.5 + 0.042ν (mV s^{-1}) (R^2 = 0.992) for MPV, I_{Pa} (μA) = 2.03 + 0.05ν (mV s^{-1}) (R^2 = 0.996) for PCM. Moreover, when examining the plot correlating the logarithm of I_{pa} and logarithm of ν (Fig. S6C and F†), linear equations were derived, and the corresponding slopes were 0.75 and 0.8, respectively. The results indicated that MPV and PCM oxidation on the CeNPs@MWCNTs/GCMFE were controlled by the kinetic adsorption process. Moreover, the E_{pa} was shifted towards the anodic side by increasing the scan rate. Plots illustrating the relationship between E_{pa} and the natural logarithm of ν were generated (Fig. S6G and H†). The corresponding linear equations between the peak potential and natural logarithm of the scan rate emerged: $E_{Pa(MPV)}$ (V) = 0.4 + 0.024 ln ν (R^2 = 0.991) and $E_{Pa(PCM)}$ (V) = 0.5 + 0.023 ln ν (R^2 = 0.989). As per the Laviron equation,[48] the values of n during the oxidation of MPV and PCM were calculated to be 2.14 and 2.2, respectively. Therefore, the results indicated that the electrochemical reactions of MPV and PCM on CeNPs@MWCNTs electrocatalyst-modified GCMFE involved two electrons and two protons.

Mechanism of detection of MPV and PCM

The electrochemical-sensing mechanisms of both drugs were proposed based on the results of the pH, sweep rate, and EIS measurements. Scheme 2 shows the possible mechanisms of the electrochemical reactions of MPV and PCM at CeNPs@MWCNTs electrocatalyst-modified GCMFE. As is known, MWCNTs are a good electron acceptor and CeNPs are a good electron donor.[49] The redox properties of CeNPs with dual oxidation states (Ce^{4+}/Ce^{3+}) co-existing on the surface may act as oxidants for biomolecule electro-oxidation.[50] They can provide a large number of reactive oxygen species and active sites and improve the electrical conductivity of the nanocatalyst materials.[51] This will increase the electrons capable of transferring from CeNPs to MWCNTs, thereby obtaining special electrochemical properties by promoting the oxidation reactions of MPV and PCM. Equal numbers of electrons and protons participated in the oxidation of both drugs, as confirmed by the pH and scan rate studies. The low R_{ct} (225 ± 13 Ω) and the increased surface area (0.86 ± 0.022 cm^2) of the CeNPs@MWCNTs/GCMFE caused the rapid transfer of electrons to the electrode. Therefore, CeNPs@MWCNTs electrocatalyst-modified GCMFE is more suitable for the simultaneous determination of MPV and PCM in practical applications.

Selective determination of MPV and PCM

The electrochemical performance of CeNPs@MWCNTs electrocatalyst-modified GCMFE towards the selective assays of MPV and PCM was monitored. A controlled AdS-SWV experiment was performed at the CeNPs@MWCNTs/GCMFE sensor, keeping the concentration of PCM (2.8 μM) fixed with a variable concentration of MPV from 8.0 to 3500 nM (Fig. S7A†). The anodic response of MPV increases linearly with the increasing addition of MPV, as can be seen in Fig. S7A† (inset). The LOD, LOQ, and sensitivity of MPV were estimated to be 8.2 nM, 27 nM, and 78.6 μA μM^{-1} cm^{-2}, respectively. Similarly, as the concentration of PCM increased from 10.0 to 2500 nM in the presence of 2.6 μM MPV, the current responses of PCM gradually increased while the peak current of MPV remained almost unchanged, which revealed that the concentration variation of PCM did not interfere with the peak current of MPV (Fig. S7B†). The sensor presented excellent analytical performance toward PCM detection with high sensitivity (77.1 μA μM^{-1} cm^{-2}) and a low LOD (10.5 nM). This demonstrated the high-resolution CeNPs@MWCNTs electrocatalyst-modified GCMFE for simultaneous detection of MPV and PCM in their binary mixture without interfering with each other.

Simultaneous determination of MPV and PCM

Simultaneous monitoring of MPV and PCM is a crucial necessity because they are co-administered for COVID-19 patients. Under optimized AdS-SWV conditions (Fig. S5†), the simultaneous determination of MPV and PCM at CeNPs@MWCNTs/GCMFE in the BRB solution (pH 6.0) was analyzed. Fig. 4A shows the voltammetric responses of the two analytes at the fabricated sensor. It shows that both the MPV and PCM peaks are well delineated, and the ΔE_{Pa} of PMV-PCM was 160 mV. Fig. 4B and C show that the current responses of MPV and PCM linearly increased with their concentrations. The analytical parameters and sensitivity using the AdS-SWV technique for both drugs are presented in Table S2.† To evaluate the performance and sensitivity of the CeNPs@MWCNTs/GCMFE sensor, it was compared with other reported electrodes for the individual-level detection of MPV and PCM (Table 1). This newly fabricated sensor displayed remarkable electrochemical performance for the simultaneous determination of MPV and PCM with low LODs of 6.0 nM and 8.6 nM, respectively, and a wide LDR from 5.0 to 5120 nM for MPV and from 8.0 to 4160 nM for PCM compared to previously modified electrodes. The following factors led to the impressive performance of the sensor that was constructed: (i) the large effective surface area has more active sites and adsorption centers; (ii) the introduction of MWCNTs effectively improves the electrical conductivity of nanoceria; and (iii) MWCNTs and nanoceria play a synergistic role to considerably improve the detection performance and sensitivity of the sensing platform.

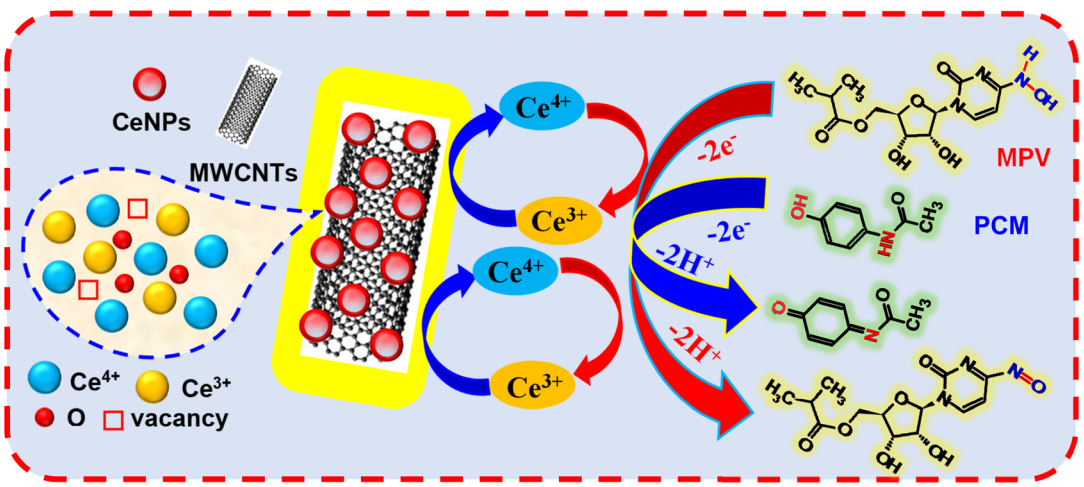

Scheme 2 The proposed electrochemical oxidation mechanism of MPV and PCM at CeNPs@MWCNTs/GCMFE.

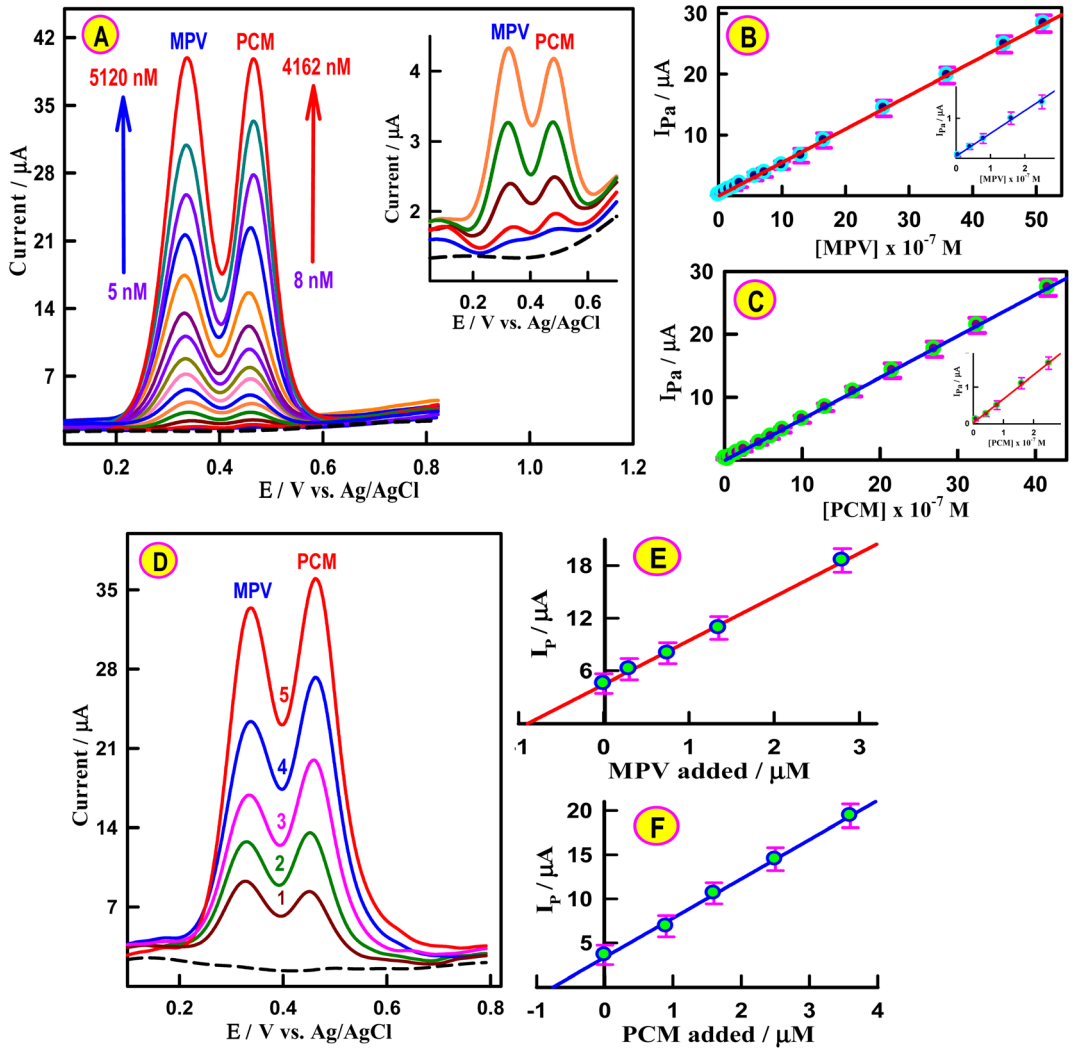

Fig. 4 (A) AdS-SW voltammograms of simultaneous determination of MPV (5.0–5120 nM) and PCM (8.0–4162 nM) CeNPs@MWCNTs/GCMFE in BRB solution (pH 6.0). (B&C) Corresponding calibration plots for MPV and PCM. (D) AdS-SW voltammograms of (1) the diluted samples of Molnupiravir-Rameda and Panadol tablets formulation and after standard additions of (2) 0.3 + 0.9, (3) 0.75 + 1.6, (4) 1.4 + 2.5, and (5) 2.8 + 3.6 µM MPV + PCM in BRB solution (pH 6.0) at CeNPs@MWCNTs/GCMFE sensor. (E and F) Corresponding linear calibration plots of peak current *vs.* concentration of added MPV and PCM. The error bar represents the standard deviation of triple measurements.

Table 1 A comparison of electrodes for the individual determination of MPV and PCM

Analyte	Electrode	LDR/µM	LOD/nM	Ref.
MPV	rGO-GCE	0.09–4.57	30	17
	Fe_3O_4/CPE	0.25–1500	50	18
	Cu-BTC@EG-PEDOT:PSS/GCE:PSS/GCE	0.1–63.3	71.3	19
	rGO-SPCE	0.152–18.272	48	20
PCM	AuNPs/MWCNT/GCE	0.09–35	30	21
	PEDOT/GO/GCE	10 – 60	570	22
	Pt/NDG	0.05–90	8.0	23
	GCE/Pd-SB	1.0–50	67	24
	γ-Fe_2O_3/CNTs	2.5–385	46	25
	ZnO/FMWCNT/CPE	0.5–13	23	26
MPV and PCM	CeNPs@MWCNTs/GCMFE	MPV: 0.005–5.12	6.0	This work
		PCM: 0.008–4.16	8.6	

Table 2 Recovery of MPV and PCM in human serum and urine samples ($n = 5$)[a]

		Serum			Urine		
Compound	Spiked (nM)	Found (nM)	Precision RSD (%)	Recovery (%)	Found (nM)	Precision RSD (%)	Recovery (%)
MPV	70	67 ± 0.15	2.1	95.7	68.5 ± 0.1	1.7	97.9
	350	345 ± 0.5	1.8	98.6	347 ± 0.4	2.3	99.1
	500	508 ± 0.3	2.4	101.6	504.5 ± 0.2	1.9	100.9
PCM	40	40.8 ± 0.12	2.2	102	39.5 ± 0.2	1.6	98.7
	160	158 ± 0.24	1.6	98.7	162 ± 0.4	2.1	101.2
	320	323 ± 0.43	1.9	100.9	321.5 ± 0.5	2.4	100.5

[a] Found: mean ± standard error.

Simultaneous analysis of MPV and PCM in real samples

Prior to testing the credibility of the proposed sensor, an examination of its repeatability, reproducibility, and stability was conducted (Fig. S8 and S9†). The simultaneous analysis of MPV and PCM in biological fluids such as human blood serum and urine samples demonstrated the practical application of the sensing electrode. Human blood serum and urine samples were obtained from the hospital of the Assiut University and used shortly after the collection. Fig. S10A† shows representative AdS-SW voltammograms for the simultaneous assay of the coexistence of MPV and PCM spiked in human serum samples. As shown in Fig. S10A† the two peaks at 0.33 V and 0.47 V correspond to the oxidation of MPV and PCM, respectively, and are used for quantification of these drugs in serum samples. Potentially interfering compounds that may be present in serum samples do not indicate any electrochemical response where the analytical peaks appear. As can be seen in Fig. S10B and C,† the oxidation peak currents of MPV and PCM are linearly proportional to their concentrations. The LOD values for MPV and PCM in the spiked serum samples were 7.2 and 10.7 nM, respectively.

The constructed sensor was successfully applied for the simultaneous analysis of the two drugs in spiked human urine samples (Fig. S11A†). Linear relationships were obtained between the peak currents and the concentrations of MPV and PCM in the urine sample (Fig. S11B and C†). The LDR, LOD, LOQ, and sensitivity were calculated and are shown in Table S3.† The calculated recovery results of the MPV and PCM concentrations in biological samples were between 97.9% and 101.2%, with RSDs lower than 2.5% (Table 2). Furthermore, the suggested AdS-SWV was utilized for monitoring MPV and PCM in the pharmaceutical products (Molnupiravir-Rameda 200 mg, Panadol 500 mg) using the constructed sensor (Fig. 4D–F). The recovery values listed in Table S4† were in the range of 96.8–102.3%. Based on these results, CeNPs@MWCNTs electrocatalyst-modified GCMFE demonstrates an excellent capability for the simultaneous electrochemical monitoring of MPV and PCM in human biological samples and commercial tablet dosage forms.

Conclusions

Sensitive sensing platforms have become an effective method to analyze biological compounds. Herein, we constructed a novel sensor based on nanoceria-decorated MWCNTs electrocatalyst (CeNPs@MWCNTs) for the simultaneous detection of antiviral drugs MPV and PCM. Morphological analysis of the modified electrode clearly revealed that the CeNPs@MWCNTs electrocatalyst was incorporated into the glassy carbon microsphere fluorolube oil paste electrode (GCMFE), which enhanced the electrochemical performance toward simultaneous detection of MPV and PCM. The electrochemical analysis studied for MPV and PCM detection experienced a good current response, which was enhanced owing to the higher surface area and improved electron transfer to the surface. Furthermore, the fabricated sensor showed excellent detection limits, 6.0 nM, 8.6 nM, linear ranges, 5.0–5120 nM and 8.0–4162 nM, and sensitivities, 78.6 and 94.3 $\mu A\ \mu M^{-1}\ cm^{-2}$, for simultaneous detection of MPV and PCM. Furthermore, the proposed sensor exhibited good repeatability, reproducibility, storage stability, and anti-interference capability toward MPV and PCM. In addition, it showed a satisfactory recovery rate in human biological fluids and pharmaceutical products. The obtained results suggested that CeNPs@MWCNT electrocatalyst-incorporated GCMs could become a prospective candidate for the construction of both solid and screen-printed electrodes in the future for the determination of MPV and PCM individually and simultaneously.

Conflicts of interest

There are no conflicts to declare.

Acknowledgements

The authors are thankful to the Deanship of Scientific Research at Najran University for funding this work under the National Research Priorities funding program grant code (NU/DRP/MRC/12/6).

References

1 M. Toots, J.-J. Yoon, R. M. Cox, M. Hart, Z. M. Sticher, N. Makhsous, R. Plesker, A. H. Barrena, P. G. Reddy and D. G. Mitchell, Characterization of orally efficacious influenza, drug with high resistance barrier in ferrets and human airway epithelia, *Sci. Transl. Med.*, 2019, **11**, 515.

2 G. R. Painter, M. G. Natchus, O. Cohen, W. Holman and W. P. Painter, Developing a direct acting, orally available antiviral agent in a pandemic: the evolution of molnupiravir as a potential treatment for COVID-19, *Curr. Opin. Virol.*, 2021, **50**, 17–22.

3 H. Ghadimi, R. M. A. Tehrani, A. S. M. Ali, N. Mohamed and S. Ab Ghani, Sensitive voltammetric determination of paracetamol by poly (4-vinylpyridine)/multiwalled carbon nanotubes modified glassy carbon electrode, *Anal. Chim. Acta*, 2013, **765**, 70–76.

4 M. T. Olaleye and B. T. J. Rocha, Acetaminophen-induced liver damage in mice: effects of some medicinal plants on the oxidative defense system, *Exp. Toxicol. Pathol.*, 2008, **59**, 319–327.

5 X. u. Chen, J. Zhu, Q. Xi and W. Yang, A high performance electrochemical sensor for acetaminophen based on single-walled carbon nanotube–graphene nanosheet hybrid films, *Sens. Actuators, B*, 2012, **161**(1), 648–654.

6 A. K. Mohiuddin, M. S. Ahmed and S. Jeon, Palladium doped α-MnO_2 nanorods on graphene as an electrochemical sensor for simultaneous determination of dopamine and paracetamol, *Appl. Surf. Sci.*, 2022, **578**, 152090.

7 J. Micallef, T. Soeiro and A. P. Jonville-Béra, COVID-19 and NSAIDs: Primum non nocere, *Therapies*, 2020, **75**, 514.

8 N. S. Leal, Y. Yu, Y. Chen, G. Fedele and L. M. Martins, Paracetamol is associated with a lower risk of COVID-19 infection and decreased ACE2 protein expression: A retrospective analysis, *Covid*, 2021, **1**, 218–229.

9 H. Ibrahim and Y. Temerk, A novel electrochemical sensor based on gold nanoparticles decorated functionalized carbon nanofibers for selective determination of xanthine oxidase inhibitor febuxostat in plasma of patients with gout, *Sens. Actuators, B*, 2021, **347**, 130626.

10 H. Ibrahim and Y. Temerk, A novel electrochemical sensor based on functionalized glassy carbon microparticles@CeO_2 core–shell for ultrasensitive detection of breast anticancer drug exemestane in patient plasma and pharmaceutical dosage form, *Microchem. J.*, 2021, **167**, 106264.

11 H. Ibrahim and Y. Temerk, Surface decoration of functionalized carbon black nanoparticles with nanosized gold particles for electrochemical sensing of diuretic spironolactone in patient plasma, *Microchem. J.*, 2022, **178**, 107425.

12 Y. A. Sharaf, S. El Deeb, A. E. Ibrahim, A. Al-Harrasi and R. A. Sayed, Two green micellar HPLC and mathematically assisted UV spectroscopic methods for the simultaneous, determination of molnupiravir and favipiravir as a novel combined COVID-19 antiviral regimen, *Molecules*, 2022, **27**, 2330.

13 T. Reçber, S. S. Timur, S. E. Kablan, F. Yalçın, T. C. Karabulut, R. N. Gürsoy, H. Eroglu, S. Kır and E. Nemutlu, A stability indicating RP-HPLC method for determination of the COVID-19 drug molnupiravir applied using nanoformulations in permeability studies, *J. Pharm. Biomed. Anal.*, 2022, **214**, 114693.

14 S. Ravisankar, M. Vasudevan, M. Gandhimathi and B. Suresh, Reversed-phase HPLC method for the estimation of acetaminophen, ibuprofen and chlorzoxazone in formulations, *Talanta*, 1998, **46**(6), 1577–1581.

15 A. H. Abdelazim, M. A. S. Abourehab, L. M. Abd Elhalim, A. A. Almrasy and S. Ramzy, Green adherent spectrophotometric determination of molnupiravir based on computational calculations; application to a recently FDA-approved pharmaceutical dosage form, *Spectrochim. Acta, Part A*, 2023, **285**, 121911.

16 R. Sandulescu, S. Mirel and R. Oprean, The development of spectrophotometric and electroanalytical methods for ascorbic acid and acetaminophen and their applications in the analysis of effervescent dosage forms, *J. Pharm. Biomed. Anal.*, 2000, **23**, 77–87.

17 S. E. Kablan, T. Reçber, G. Tezel, S. S. Timur, C. Karabulut, T. C. Karabulut, H. Eroglu, S. Kır and E. Nemutlu, Voltammetric sensor for COVID-19 drug Molnupiravir on modified glassy carbon electrode with electrochemically reduced graphene oxide, *J. Electroanal. Chem.*, 2022, **920**, 116579.

18 K. Vural, S. Karakaya, D. G. Dilgin, H. I. Gokçel and Y. Dilgin, Voltammetric determination of Molnupiravir used in treatment of the COVID-19 at magnetite nanoparticle modified carbon paste electrode, *Microchem. J.*, 2023, **184**, 108195.

19 N. Erk, W. Bouali, M. Mehmandoust and M. Soylak, An electrochemical sensor for molnupiravir based on a metal-organic framework composited with poly(3,4- ethylene dioxythiophene): Poly(styrene sulfonate), *ChemistrySelect*, 2022, **7**, e202203325.

20 A. Nabil, H. A. M. Hendawy, R. Abdel-Salam, R. M. Ahmed, A. Shawky, S. Emara and N. Ibrahim, A green voltammetric determination of molnupiravir using a disposable screen-printed reduced graphene oxide electrode: application for pharmaceutical dosage and biological fluid forms, *Chemosensors*, 2023, **11**, 471.

21 W. Si, W. Lei, Z. Han, Y. Zhang, Q. Hao and M. Xia, Electrochemical sensing of acetaminophen based on poly(3, 4-ethylenedioxythiophene)/graphene oxide composites, *Sens. Actuators, B*, 2014, **193**, 823–829.

22 N. Adhoum, L. Monser, M. Toumi and K. Boujlel, Determination of naproxen in pharmaceuticals by differential pulse voltammetry at a platinum electrode, *Anal. Chim. Acta*, 2003, **495**(1–2), 69–75.

23 N. S. Anuar, W. J. Basirun, M. Ladan, Md. Shalauddin and M. S. Mehmood, Fabrication of platinum nitrogen-doped graphene nanocomposite modified electrode for the electrochemical detection of acetaminophen, *Sens. Actuators, B*, 2018, **266**, 375–383.

24 M. A. Hefnawy, S. S. Medany, S. A. Fadlallah, R. M. El-Sherif and S. S. Hassan, Novel self-assembly Pd(II)-schiff base complex modified glassy carbon electrode for electrochemical detection of paracetamol, *Electrocatalysis*, 2022, **13**, 598–610.

25 X.-Q. Cai, K. Zhu, B.-T. Liu, Q.-Y. Zhang, Y.-H. Luo and D.-E. Zhang, γ-Fe2O3/CNTs composites for electrochemical detection of paracetamol: synthesis, phase transition and enhanced properties, *J. Electrochem. Soc.*, 2021, **168**, 057511.

26 M. Kumar, B. E. K. Swamy, S. Reddy, W. Zhao, S. Chetana and V. G. Kumar, ZnO/functionalized MWCNT and Ag/functionalized MWCNT modified carbon paste electrodes for the determination of dopamine, paracetamol and folic acid, *J. Electroanal. Chem.*, 2019, **835**, 96–105.

27 R. M. K. Mohamed, S. H. Mohamed, A. M. Asran, I. H. Alsohaimi, H. M. A. Hassan, H. Ibrahim and M. M. El-Wekil, Synergistic effect of gold nanoparticles anchored on conductive carbon black as an efficient electrochemical sensor for sensitive detection of anti-COVID-19 drug Favipiravir in absence and presence of co-administered drug Paracetamol, *Microchem. J.*, 2023, **190**, 108696.

28 S. Karakaya and Y. Dilgin, Disposable and sensitive electrochemical determination of molnupiravir at a pencil graphite electrode (PGE) by differential pulse voltammetry (DPV), *Anal. Lett.*, 2023, 1–14.

29 R. M. K. Mohamed, S. H. Mohamed, A. M. Asran, I. H. Alsohaimi, H. M. A. Hassan and H. Ibrahim, Carbon microspheres uniformly decorated with ceria nanoparticles as an ultrasensitive platform for electrochemical sensing of antihypertensive drug lacidipine in patient plasma and pharmaceutical formulation, *Microchem. J.*, 2023, **187**, 108.

30 H. M. Ali, I. H. Alsohaimi, A. A. Nayl, A. A. Essawy, M. Gamal and H. Ibrahim, A new ultrasensitive platform based on f-GCNFs@nano-CeO_2 core-shell nanocomposite for electrochemical sensing of oxidative stress biomarker 3-nitrotyrosine in presence of uric acid and tyrosine, *Microchem. J.*, 2022, **183**, 108068.

31 H. Ibrahim and Y. Temerk, Synergistic electrocatalytic activity of In_2O_3@FMWCNTs nanocomposite for electrochemical quantification of dobutamine in clinical patient blood and in injection dosage form, *Talanta*, 2020, **208**, 120362.

32 Y. Temerk and H. Ibrahim, Fabrication of a novel electrochemical sensor based on Zn–In_2O_3 nanorods coated glassy carbon microspheres paste electrode for square wave voltammetric determination of neuroprotective hibifolin in biological fluids and in the flowers of hibiscus vitifolius, *J. Electroanal. Chem.*, 2016, **782**, 9–18.

33 M. Ibrahim, H. Ibrahim, N. B. Almandil, M. A. Sayed, A.-N. Kawde and Y. Aldaqdouq, A novel platform based on Au-CeO_2@MWCNT functionalized glassy carbon microspheres for voltammetric sensing of valrubicin as bladder anticancer drug and its interaction with DNA, *Electroanalysis*, 2020, **32**, 2146–2155.

34 H. Ibrahim, M. Ibrahim and Y. Temerk, A novel megestrol acetate electrochemical sensor based on conducting functionalized acetylene black–CeO_2NPs nanohybrids decorated glassy carbon microspheres, *Talanta*, 2019, **200**, 324–332.

35 H. Maseed, V. M. R. Yenugu, S. S. Devarakonda, S. Petnikota, M. Gajulapalli and V. V. S. S. Srikanth, Peroxidase-like Fe_3O_4 nanoparticle/few-layered graphene composite for electrochemical detection of dopamine, ascorbic acid, and uric acid, *ACS Appl. Nano Mater.*, 2023, **6**, 18531–18538.

36 C. C. Tang, Y. Bando, B. D. Liu and D. Golberg, Cerium oxide nanotubes prepared from cerium hydroxide nanotubes, *Adv. Mater.*, 2005, **17**, 3005–3009.

37 J. Dong, X. Wang, F. Qiao, P. Liu and S. Ai, Highly sensitive electrochemical stripping analysis of methyl parathion at MWCNTs–CeO_2–Au nanocomposite modified electrode, *Sens. Actuators, B*, 2013, **186**, 774–780.

38 A. S. Razavian, S. M. Ghoreishi, A. S. Esmaeily, M. Behpour, L. M. A. Monzon and J. M. D. Coey, Simultaneous sensing of L-tyrosine and epinephrine using a glassy carbon electrode modified with nafion and CeO_2 nanoparticles, *Microchim. Acta*, 2014, **181**, 1947–1955.

39 M. Shalauddin, S. Akhter, W. J. Basirun, S. Bagheri, N. S. Anuar and M. R. Johan, Hybrid nanocellulose/f-MWCNTs nanocomposite for the electrochemical sensing of diclofenac sodium in pharmaceutical drugs and biological fluids, *Electrochim. Acta*, 2019, **304**, 323–333.

40 J. Wang, U. A. Kirgöz, J. W. Mo, J. Lu and A. Muck, Glassy carbon paste electrodes, *Electrochem. Commun.*, 2001, **3**, 203.

41 J. Barek, A. Muck, J. Wang and J. Zima, Study of voltammetric determination of carcinogenic 1-Nitropyrene and 1-Aminopyrene using a glassy carbon paste electrode, *Sensors*, 2004, **4**, 47–57.

42 R. Rao, Q. Zhang, H. Liu, H. Yang, Q. Ling, M. Yang, A. Zhang and W. Chen, Enhanced catalytic performance of CeO_2 confined inside carbon nanotubes for dehydrogenation of ethylbenzene in the presence of CO_2, *J. Mol. Catal. A: Chem.*, 2012, **363–364**, 283–290.

43 S. Shankar, N. S. K. Gowthaman and S. A. John, Synthesis of albumin capped gold nanoparticles and their direct attachment on glassy carbon electrode for the determination of nitrite ion, *J. Electroanal. Chem.*, 2018, **828**, 33–40.

44 T. Gan, Z. K. Wang, Z. X. Shi, D. Y. Zheng, J. Y. Sun and Y. M. Liu, Graphene oxide reinforced core shell structured Ag@Cu_2O with tunable hierarchical morphologies and their morphology dependent electrocatalytic properties for bio-sensing applications, *Biosens. Bioelectron.*, 2018, **112**, 23–30.

45 F. Kaedi, Z. Yavari, M. Asmaei, A. R. Abbasian and M. Noroozifar, Ethanol electrooxidation on high-performance mesoporous $ZnFe_2O_4$-supported palladium nanoparticles, *New J. Chem.*, 2019, **43**, 3884.

46 H. Ibrahim and Y. Temerk, A novel disposable electrochemical sensor based on modifying graphite pencil lead electrode surface with nanoacetylene black for simultaneous determination of antiandrogens flutamide and cyproterone acetate, *J. Electroanal. Chem.*, 2020, **859**, 113836.

47 P. C. Pwavodi, V. H. Ozyurt, S. Asir and M. Ozsoz, Electrochemical sensor for determination of various phenolic compounds in wine samples using Fe_3O_4

nanoparticles modified carbon paste electrode, *Micromachines*, 2021, **12**, 312.

48 L. Yang, B. Zhang, B. Xu, F. Zhao and B. Zeng, Ionic liquid functionalized 3D graphene carbon nanotubes-AuPd nanoparticles-molecularly imprinted copolymer based paracetamol electrochemical sensor: Preparation, characterization and application, *Talanta*, 2021, **224**, 121845.

49 A. Mourya, B. Mazumdar and S. K. Sinha, Application of CeO_2-MWCNTs nanocomposite for heavy metal ion detection in aqueous solutions by electrochemical technique, *Cleaner Mater.*, 2021, **2**, 100021.

50 M. Melchionna, M. Bevilacqua and P. Fornasiero, The electrifying effects of carbon-CeO_2 interfaces in (electro) catalysis, *Mater. Today Adv.*, 2020, **6**, 100050.

51 F. Cao, Q. Dong, C. Li, D. Kwak, Y. Huang, D. Song and Y. u. Lei, Sensitive and selective electrochemical determination of L-cysteine based on cerium oxide nanofibers modified screen printed carbon electrode, *Electroanalysis*, 2018, **30**, 1133–1139.